◇ Monograph Excerpt ◇

Matter Antimatter Fluctuations

search, discovery and analysis of Bs flavor oscillations

Nuno Leonardo

Complete work published as:
Analysis of B_s oscillations at CDF, MIT Thesis (2006)
Matter antimatter fluctuations, Monograph, LAP Lambert (2011)

Chapter 12

Constraining the CKM parameters

The precise Δm_s measurement is incorporated as a constraint to the unitarity triangle, together with other experimenal and theoretical inputs, in an inference framework for the CKM matrix elements. The theory impact of the measurement is estimated.

12.1 Likelihood technique

A global fit to the CKM matrix elements may be performed using several methods [82, 83, 84, 85]. These treat in different ways the available information on the experimental and theoretical uncertainties. We employ a Bayesian approach to construct a global inference function, from which probability intervals for the relevant parameters may be derived. In implementing our code we follow the general method documentation [82]. The uncertainties are described in terms of PDFs which quantify the confidence on the values of the involved variables.

We first motivate the procedure for a single constraint; a more general description will follow. The oscillation frequencies of the neutral B meson systems can be related, within the SM, to the CKM parameters $\bar{\rho}$ and $\bar{\eta}$ through an equation of the type

$$(1-\bar{\rho})^2 + \bar{\eta}^2 = c\,, \tag{12.1}$$

where c is a quantity formed of the experimentally measured Δm ($c \propto \Delta m_d, \Delta m_s^{-1}$), and of other theoretically determined parameters.

In the ideal case where c would be perfectly known, the constraint expressed by (12.1) would result in a curve in the $(\bar{\rho}, \bar{\eta})$ plane, *i.e.* a circle of radius $\sqrt{c}$. The PDF describing our beliefs in the $\bar{\rho}$ and $\bar{\eta}$ values would be

$$f(\bar{\rho}, \bar{\eta}|c) = \delta((1-\bar{\rho})^2 + \bar{\eta}^2 - c)\,. \tag{12.2}$$

The points in the circumference would appear equally likely. This would remain so in the absence of other experimental piece of information, or theoretical prejudice, which might exclude points outside a determined *physical region*, or in general lead to the assignment of different weights to the various points.

In a realistic case c is not known exactly, the available knowledge about its value being contained in a corresponding PDF, $f(c)$. This way, instead of a single circle, there is in reality an infinite collection of curves, each having a weight $f(c)$. The expected values for $\bar{\rho}$ and $\bar{\eta}$ are thus obtained from

$$f(\bar{\rho},\bar{\eta}) = \int f(\bar{\rho},\bar{\eta}|c)\; f(c)\; dc\,. \tag{12.3}$$

Supposing a best experimental estimate for c would be given by $\hat{c}$, with uncertainty σ_c, and assuming a Gaussian distribution, the previous equation would take the form

$$\begin{aligned} f(\bar{\rho},\bar{\eta}) &= \int \delta((1-\bar{\rho})^2+\bar{\eta}^2-c)\frac{1}{\sqrt{2\pi}\sigma_c}e^{-\frac{1}{2}\left(\frac{c-\hat{c}}{\sigma_c}\right)^2}\; dc \\ &= \frac{1}{\sqrt{2\pi}\sigma_c}e^{-\frac{1}{2}\left(\frac{(1-\bar{\rho})^2-\bar{\eta}^2-\hat{c}}{\sigma_c}\right)^2}\,. \end{aligned} \tag{12.4}$$

In a more general case, c may be formed from various input quantities $\{x_i\}$, denoted by $\mathbf{x}$, and generally described by a joint PDF $f(\mathbf{x})$; when the various x_i can be considered independent, the joint distribution simplifies to $f(\mathbf{x}) \sim \prod_i f(x_i)$. Denoting by $c(\mathbf{x})$ the dependency of c on the input quantities $\mathbf{x}$, $f(c)$ can generally be obtained as

$$f(c) = \int f(\mathbf{x})\delta(c-c(\mathbf{x}))\; d\mathbf{x}\,. \tag{12.5}$$

We describe now more generally the procedure employed in this analysis. It involves the construction of a global inference, $\mathcal{L}$, relating $\bar{\rho}$, $\bar{\eta}$, the constraints $\mathbf{c} = \{c_j\}_{j=1}^{M}$, and the parameters $\mathbf{x} = \{x_i\}_{i=1}^{N}$. The various constraints $\mathbf{c}$, standing for Δm_d, $\Delta m_s/\Delta m_d$, ϵ_K, $|V_{ub}/V_{cd}|$, $\sin 2\beta$, may be expressed as

$$c_j = c_j(\bar{\rho},\bar{\eta};\mathbf{x})\,, \tag{12.6}$$

where the parameters $\mathbf{x}$ denote here all experimentally measured and theoretically calculated quantities on which $\mathbf{c}$ depends. The set of measured constraint values is represented by $\hat{\mathbf{c}} = \{\hat{c}_j\}_{j=1}^{M}$.

Making use of Bayes's theorem, we obtain

$$\begin{aligned} \mathcal{L}(\bar{\rho},\bar{\eta},\mathbf{c},\mathbf{x}|\hat{\mathbf{c}}) &\propto f(\hat{\mathbf{c}}|\bar{\rho},\bar{\eta},\mathbf{c},\mathbf{x})\cdot f(\mathbf{c},\mathbf{x},\bar{\rho},\bar{\eta}) \\ &\propto f(\hat{\mathbf{c}}|\mathbf{c})\cdot f(\mathbf{c}|\mathbf{x},\bar{\rho},\bar{\eta})\cdot f(\mathbf{x},\bar{\rho},\bar{\eta}) \\ &\propto f(\hat{\mathbf{c}}|\mathbf{c})\cdot \delta(\mathbf{c}-\mathbf{c}(\mathbf{x},\bar{\rho},\bar{\eta}))\cdot f(\mathbf{x})\cdot f_0(\bar{\rho},\bar{\eta})\,. \end{aligned} \tag{12.7}$$

Here $f_0(\bar{\rho}, \bar{\eta})$ is the *prior* distribution for $\bar{\rho}, \bar{\eta}$, which we take as uniform; $f(\mathbf{x})$ denotes similarly the prior joint PDF for parameters $\mathbf{x}$. In the derivation we have noted that c_j are unequivocally determined, within the SM, from the values of $\bar{\rho}$, $\bar{\eta}$, and $\mathbf{x}$, and that $\hat{\mathbf{c}}$ depends on those parameters only through $\mathbf{c}$. Considering the independence of the various quantities, (12.7) becomes

$$\mathcal{L}(\bar{\rho}, \bar{\eta}, \mathbf{x}) \;\propto\; \prod_{j=1,M} f(\hat{c_j}|c_j(\bar{\rho}, \bar{\eta}, \mathbf{x})) \times \prod_{i=1,N} f_i(x_i) \;, \tag{12.8}$$

where the constraints imposed by the δ-functions in the previous expression are assumed, and the prior, constant f_0 distribution was also omitted.

The relation (12.8) constitutes our sought-after global inference. Within the framework of Bayes statistics, and upon normalization, the left-hand side of the relation is the *posterior* PDF for the argument parameters. The probability distribution for any of the involved parameters can be achieved by integration over the remaining, sometimes also called *nuisance*, quantities.

In a Bayesian approach the various uncertainties are treated in a similar fashion, such that there is no conceptual distinction between those due to random fluctuations in the measurements, those about the parameters of the theory, or those associated to systematics of parameters known but with limited accuracy. Indeed, a systematic uncertainty on a parameter on which the measured constraints depend may be handled by adding the parameter to the collection $\mathbf{x}$.

We consider two models for describing the uncertainties. A Gaussian model is chosen when the uncertainty is dominated by statistical effects, or there are many contributions to the systematic uncertainty, so that the central limit theorem applies. Otherwise, a uniform distribution is used for the uncertainty. When both Gaussian and flat uncertainty components are available for a parameter, the resulting PDF is obtained by convoluting the two distributions. That is, for an observable parameter x of true value $\bar{x}$, with Gaussian and uniform uncertainty components, σ_g, σ_u, one has for the parameter and its PDF, $f(x)$,

$$\begin{aligned} x &= \bar{x} + x_g + x_u \;, \\ f(x) &= \delta(x - \bar{x}) \otimes \mathrm{Gaus}(x|\sigma_g) \otimes \mathrm{Unif}(x|\sigma_f) \;. \end{aligned} \tag{12.9}$$

Besides the constraints themselves, we classify the involved parameters into two categories: *(i) varied*, for which we construct PDFs, and which are what we have been denoting by $\mathbf{x}$ (*e.g.* the top mass); and *(ii) fixed*, which are taken as constant (*e.g.* the W mass).

Joint PDF for $(\bar{\rho}, \bar{\eta})$ and other *posterior* probabilities

The combined probability distribution for $\bar{\rho}$ and $\bar{\eta}$ is obtained by integrating (12.8) over the (here *nuisance*) parameters $\mathbf{x}$,

$$\mathcal{L}(\bar{\rho}, \bar{\eta}) \;\; \propto \;\; \int \prod_{j=1,M} f(\hat{c_j}|c_j(\bar{\rho}, \bar{\eta}, \{x_i\})) \times \prod_{i=1,N} f_i(x_i)\; dx_i \;\; \times f_0(\bar{\rho}, \bar{\eta})\; . \tag{12.10}$$

The integration is performed using Monte Carlo methods. The normalization can then be trivially performed, and all moments can also be easily computed. This expression shows explicitly that whereas *a priori* all values of $\bar{\rho}$ and $\bar{\eta}$ are equally likely by assumption, *i.e.* $f_0(\bar{\rho}, \bar{\eta}) = \text{const.}$, *a posteriori* the probability clusters in a region of maximal likelihood.

The probability regions in the $(\bar{\rho}, \bar{\eta})$ plane are constructed from the PDF obtained in (12.10). These are called *highest posterior density* regions, and are defined such that $\mathcal{L}(\bar{\rho}, \bar{\eta})$ is higher everywhere inside the region than outside,

$$P_w := \{z = (\bar{\rho}, \bar{\eta}) \;\; : \;\; \int_{P_w} \mathcal{L}(z) dz = w;\;\; \mathcal{L}(z') < \min_{P_w} \mathcal{L}(z), \forall_{z' \notin P_w}\}\; . \tag{12.11}$$

The single parameter PDF can also be obtained in the same fashion. For example, the PDF for $\bar{\rho}$ is obtained as

$$\mathcal{L}(\bar{\rho}) \;\; \propto \;\; \int \mathcal{L}(\bar{\rho}, \bar{\eta})\; d\bar{\eta}\; , \tag{12.12}$$

from which its expected value can be calculated together with the corresponding highest posterior density intervals.

A similar procedure could be in principle used in order to obtain the PDF for other desired parameters. Alternatively, one may use the probability function for transformed variables; *i.e.*, that for $\mathbf{u}(\mathbf{x})$ one has $f(\mathbf{u}) = f(\mathbf{x})|\partial \mathbf{x}/\partial \mathbf{u}|$, where the last factor denotes the Jacobian. This way, the PDF for a parameter x is effectively obtained through a weighted integration over either $\bar{\rho}$ or $\bar{\eta}$; for instance,

$$\mathcal{L}(x) \;\; \propto \;\; \int \mathcal{L}(x, \bar{\eta})\; d\bar{\eta} \;\; = \;\; \int \mathcal{L}(\bar{\rho}, \bar{\eta}) \;\; \left|\frac{d\bar{\rho}}{dx}\right| \;\; d\bar{\eta}\; , \tag{12.13}$$

where $\mathcal{L}(\bar{\rho}, \bar{\eta})$ has been computed in (12.10) above. Besides the probability distribution for $\bar{\rho}$ and $\bar{\eta}$, we are also interested in obtaining the *posterior* distribution for the Δm_s observable itself. The latter may be obtained as

$$\begin{aligned} \mathcal{L}(\Delta m_s) \;\; &= \;\; \int \mathcal{L}(\bar{\rho}, \bar{\eta}) \left|\frac{d\bar{\eta}}{d\,\Delta m_s}\right| d\bar{\rho} \\ &= \;\; \int \mathcal{L}(\bar{\rho}, \bar{\eta})\, \frac{1}{\Delta m_s} \frac{(1-\bar{\rho})^2 + \bar{\eta}^2}{2\bar{\eta}}\, d\bar{\rho}\; , \end{aligned} \tag{12.14}$$

where the Jacobian has been calculated from the constraint (12.20).

12.2 Constraints

12.2.1 Neutral B meson mixing

Flavor oscillations in the neutral B meson systems are described within the SM by the electroweak box diagrams of Figure 2.2, which are dominated by t quark exchange. The evaluation of corresponding effective Hamiltonian matrix elements, following the formalism presented in Section 2.1, leads to the following expression for the oscillation frequencies (with $q = s, d$)

$$\Delta m_q = \frac{G_F^2}{6\pi^2} m_W^2 \eta_{B_q} m_{B_q} B_{B_q} f_{B_q}^2 S_0(x_t) |V_{tq}^* V_{tb}|^2 \,. \tag{12.15}$$

Here G_F is the Fermi constant; η_{B_q} is a QCD correction factor calculated in NLO; m_{B_q} and m_W are the B_q meson and W boson masses. The Inami-Lim function is given by

$$S_0(x_t) \;=\; x_t \left[\frac{1}{4} + \frac{9}{4}\frac{1}{1-x_t} - \frac{3}{2}\frac{1}{(1-x_t)^2}\right] - \frac{3}{2}\left[\frac{x_t}{1-x_t}\right]^3 \ln x_t, \tag{12.16}$$

which describes the $|\Delta B| = 2$ transition amplitude in the absence of strong interaction, with $x_t \equiv m_t^2/m_W^2$ denoting the ratio of the t quark and W boson masses.

The dominant uncertainties in (12.15) come from the evaluation of the hadronic quantities: the B meson decay constant, f_{B_q}, and the bag factor, B_{B_q}, which parameterize the value of the hadronic matrix element (2.66). The ratio of these hadronic quantities for the two systems,

$$\xi_\Delta = \frac{f_{B_s}\sqrt{B_{B_s}}}{f_{B_d}\sqrt{B_{B_d}}} \,, \tag{12.17}$$

is more accurately obtained from lattice QCD calculations [13].

Δm_d constraint

Expressing (12.15) above, for the B^0 case, in terms of the Wolfenstein parameters, we obtain

$$\Delta m_d = \frac{G_F^2 m_W^2}{6\pi^2} A^2\lambda^6[(1-\bar\rho)^2 + \bar\eta^2] m_{B_d} \frac{f_{B_s}^2 B_{B_s}}{\xi_\Delta^2} \eta_{B_d} S(x_t) \,. \tag{12.18}$$

Note that ξ_Δ and $f_{B_s}\sqrt{B_{B_s}}$ are used instead of $f_{B_d}\sqrt{B_{B_d}}$, which renders the constraint more effective [82]. in view of current parameter uncertainties.

The quantities with dominant uncertainties in (12.18) are $f_{B_s}\sqrt{B_{B_s}}$, ξ_Δ, A and λ, which are varied parameters of the fit. A Gaussian constraint is implemented in the global likelihood,

$$e^{-\frac{1}{2}\left(\frac{\Delta m_d - \widehat{\Delta m_d}}{\sigma_{\Delta m_d}}\right)^2} \,, \tag{12.19}$$

fixed parameters	
G_F $[\mathrm{GeV}^{-2}\hbar^3\mathrm{c}^3]$	1.16637×10^{-5}
M_W $[\mathrm{GeV/c^2}]$	80.425 ± 0.038
f_K [GeV]	0.1598 ± 0.0015
m_K $[\mathrm{GeV/c^2}]$	0.49765 ± 0.00002
Δm_K $[\mathrm{GeV/c^2}]$	$(3.483 \pm 0.006) \times 10^{-15}$
η_{tt}	0.574 ± 0.004
m_{B^0} $[\mathrm{GeV/c^2}]$	5.2794 ± 0.0005
η_B	0.55 ± 0.007
m_{B_s} $[\mathrm{GeV/c^2}]$	5.3696 ± 0.0024

Table 12.1: Input values of *fixed* parameters.

where Δm_d is provided by the r.h.s. of (12.18), while $\widehat{\Delta m_d}$ and $\sigma_{\Delta m_d}$ denote the experimentally measured values.

Δm_s constraint

A more powerful constraint of the side $|V_{td}|/(\lambda|V_{cb}|)$ of the unitarity triangle is obtained from the ratio of oscillation frequencies. The constraint associated to Δm_s is expressed, from (12.17) and (12.18), as

$$\Delta m_s = \Delta m_d \frac{m_{B_s}}{m_{B_d}} \xi_\Delta^2 \frac{(1-\lambda^2/2)^2}{\lambda^2} \frac{1}{(1-\bar{\rho})^2+\bar{\eta}^2}\,, \tag{12.20}$$

where Δm_d is here taken as an experimental input.

The parameters with dominant uncertainties in (12.20) are ξ_Δ, A and λ, which are varied parameters of the fit. The constraint is implemented via the likelihood ratio, $\mathcal{R}$ as given by (12.28), after accessing the experimentally measured amplitude point $(\mathcal{A}, \sigma_\mathcal{A})$ associated to the frequency value obtained by evaluating the r.h.s. of (12.20).

12.2.2 Other constraints and input

$|V_{ub}|/|V_{cb}|$ constraint

The CKM matrix elements $|V_{ub}|$ and $|V_{cb}|$ are measured from both inclusive and exclusive semileptonic B decays. $|V_{cb}|$ is more accurately obtained from exclusive $B \to D^{(*)} l \bar{\nu}_l$ and inclusive semileptonic b decays to charm. The extraction of $|V_{ub}|$ from charmless semileptonic inclusive decays, $B \to X_u l \bar{\nu}_l$, is performed but not without complications. In effect,

varied parameters	
$\|V_{cb}\|_{\text{incl.}}$	$(41.6 \pm 0.7) \times 10^{-3}$
$\|V_{cb}\|_{\text{excl.}}$	$(41.3 \pm 1.0 \pm 1.8) \times 10^{-3}$
$\|V_{ub}\|_{\text{incl.}}$	$(43.9 \pm 2.0 \pm 2.7) \times 10^{-4}$
$\|V_{ub}\|_{\text{excl.}}$	$(38.0 \pm 2.7 \pm 4.7) \times 10^{-4}$
$\|V_{us}\|$	0.2258 ± 0.0014
$\|\epsilon_K\|$	$(2.280 \pm 0.017) \times 10^{-3}$
B_K	$0.79 \pm 0.04 \pm 0.09$
$\overline{m}_c$ [GeV/c^2]	1.3 ± 0.1
$\overline{m}_t$ [GeV/c^2]	161.5 ± 3.0
η_{cc}	1.38 ± 0.53
η_{ct}	0.47 ± 0.04
$\sin 2\beta$	0.687 ± 0.032
Δm_d [$\hbar$/c^{2}ps^{-1}]	0.507 ± 0.005
$f_{B_s}\sqrt{B_{B_s}}$ [GeV]	0.276 ± 0.038
ξ_Δ	$1.21 \pm 0.04 \pm 0.06$
Δm_s	amplitude scan

Table 12.2: Input values of *varied* parameters; the first and (when available) the second uncertainties are treated respectively by Gaussian and flat models.

experimental techniques aimed at suppressing the large $B \to X_c l \bar{\nu}_l$ background result in the introduction of additional theoretical uncertainties. Among the determinations from exclusive decays, such as $B \to \pi l \bar{\nu}_l$, $B \to \rho l \bar{\nu}_l$, $B \to w l \bar{\nu}_l$, and $B \to \eta l \bar{\nu}_l$, the former is the most advanced, as both experimental and lattice calculations are under best control.

In terms of the re-scaled Wolfenstein parameters, the ratio $|V_{ub}|/|V_{cb}|$ is expressed as the constraint

$$\left|\frac{V_{ub}}{V_{cb}}\right| = \frac{\lambda}{1-\lambda^2/2}\sqrt{\bar{\rho}^2+\bar{\eta}^2}\ . \tag{12.21}$$

Both Gaussian and flat uncertainties are computed, and a corresponding convoluted PDF is employed in the implementation of the constraint.

$|\epsilon_K|$ constraint

The kaon systems provide various possible constraints, from mixing, CP violation, and rare decays. Only indirect CP violation is used in the CKM fit, since the corresponding matrix elements can be obtained by lattice QCD with controlled systematic uncertainties. The measurement of indirect CP violation in the neutral K system is expressed through the parameter ϵ_K.

In terms of the Wolfenstein parameters, $|\epsilon_K|$ is given by

$$\begin{aligned} |\epsilon_K| &= \frac{G_F^2 f_K^2 m_K m_W^2}{6\sqrt{2}\pi^2 \Delta m_K} B_K A^2 \lambda^6 \bar{\eta} [-\eta_1 x_c + A^2\lambda^4 \left(1-\bar{\rho}-\left(\bar{\rho}^2+\bar{\eta}^2\right)\lambda^2\right)\eta_2 S_0(x_t) \\ &+ \eta_3 S_0(x_c, x_t)]\ . \end{aligned} \tag{12.22}$$

The short distance QCD corrections are codified in the coefficients η_1, η_2 and η_3, and are functions of the charm and top quark masses, and of the QCD scale parameter $\Lambda_{\rm QCD}$; the η_i have been calculated in next to leading order (NLO) QCD. The Inami-Lim functions, which describe the $|\Delta S| = 2$ transition amplitude in the absence of strong interactions, are given by

$$\begin{aligned} S_0(x_t) &= x_t\left[\frac{1}{4}+\frac{9}{4}\frac{1}{1-x_t}-\frac{3}{2}\frac{1}{(1-x_t)^2}\right]-\frac{3}{2}\left[\frac{x_t}{1-x_t}\right]^3 \ln x_t\,, \\ S_0(x_c, x_t) &= -x_c \ln x_c + x_c\left[\frac{x_t^2-8x_t+4}{4(1-x_t)^2}\ln x_t + \frac{3}{4}\frac{x_t}{x_t-1}\right]\,, \quad x_q \equiv \frac{m_q^2}{m_W^2}\ . \end{aligned} \tag{12.23}$$

The parameters with dominant uncertainties are B_K, η_1, η_3, m_c and m_t. A Gaussian constraint is implemented for $|\epsilon_K|$.

$\sin 2\beta$ constraint

A direct determination of the angles of the unitarity triangle can be achieved via measurements of CP asymmetries in various B decays. In $b \to c\bar{c}s$ transitions the time dependent

CP violation parameters measured from the interference between decays with and without mixing coincide with $\sin 2\beta$ to a very good approximation. The theoretically cleanest cases are the $B^0 \to J/\psi K_{S,L}$ decays, while the world average uses additional measurements involving $\psi(2S)K_S$, $\chi_{c1}K_S$ and $J/\psi K^{*0}$ ($K^{*0} \to K_S\pi^0$) final states. In $b \to c\bar{c}d$ decays, such as $B^0 \to J/\psi\pi^0$ and $B^0 \to D^{(*)}D^{(*)}$, unknown contributions from penguin-type diagrams compromise the clean extraction of $\sin 2\beta$, and consequently are not taken into account in its average used for the CKM fit.

In terms of the re-scaled Wolfenstein parameters the constraint is expressed as

$$\sin 2\beta \;=\; \frac{2\bar{\eta}(1-\bar{\rho})}{\bar{\eta}^2 + (1-\bar{\rho})^2}\,, \tag{12.24}$$

being free of hadronic uncertainties. A Gaussian constraint is implemented for $\sin 2\beta$.

The input values employed in the fit, for both fixed and varied parameters, are specified in Tables 12.1 and 12.2. The form of the constraints was also illustrated in Figures 2.4 and 2.5.

12.3 Making use of the Δm_s amplitude information

A generic constraint is implemented in the fit from the measured central value and uncertainty of the associated experimental observable. For implementing the Δm_s constraint, however, a more complete set of information about the degree of exclusion is used. Such information is contained in the full amplitude scan (or equivalently in the likelihood ratio), allowing the available information on Δm_s to be thoroughly employed, even before a definitive measurement had been achieved. The use of the amplitude measurements in the probed frequency spectrum effectively amounts to employing the Δm_s likelihood profile, as we shall see next. This provides more thorough information than just the frequency point which maximizes the likelihood, along with confidence bounds, and it is applicable regardless of whether or not a well defined, significant maximum has been found.

The measured values of the amplitude and its uncertainty, $\mathcal{A}$ and $\sigma_{\mathcal{A}}$, may be used to derive [33], in the Gaussian approximation, the log-likelihood function, $\Delta \ln \mathcal{L}^{\infty}(\Delta m_s)$, referenced to its value for an infinite oscillation frequency,

$$\Delta \ln \mathcal{L}^{\infty}(\Delta m_s) \;=\; \ln \mathcal{L}(\infty) - \ln \mathcal{L}(\Delta m_s) \;=\; \left(\frac{1}{2} - \mathcal{A}\right)\frac{1}{\sigma_{\mathcal{A}}^2}\,. \tag{12.25}$$

The expected average log-likelihood value for the cases where the probe frequency corresponds to the true oscillation frequency of the system (*mixing* case) or is far from it (*no-mixing* case), which are characterized respectively by unit and zero expected amplitude values, are given

by

$$\Delta \ln \mathcal{L}^{\infty}(\Delta m_s)_{\rm mix} \;=\; -\frac{1}{2}\frac{1}{\sigma_{\mathcal{A}}^2}\,, \tag{12.26}$$

$$\Delta \ln \mathcal{L}^{\infty}(\Delta m_s)_{\rm nomix} \;=\; +\frac{1}{2}\frac{1}{\sigma_{\mathcal{A}}^2}\,. \tag{12.27}$$

The log-likelihood difference, according to the central limit theorem of likelihood theory, is χ^2-distributed, $\Delta \ln \mathcal{L} = \frac{1}{2}\chi^2$. We therefore translate the amplitude scan into the likelihood ratio (see (11.18)) which results in

$$\mathcal{R}(\Delta m_s) \;=\; e^{-\Delta \ln \mathcal{L}^{\infty}(\Delta m_s)} \;=\; \frac{\mathcal{L}(\Delta m_s)}{\mathcal{L}(\infty)} \;=\; e^{-\frac{\frac{1}{2}-\mathcal{A}(\Delta m_s)}{\sigma_{\mathcal{A}}^2(\Delta m_s)}}\,. \tag{12.28}$$

We re-state that the exponent in (12.28) corresponds to the χ^2, or log-likelihood, difference between the cases where an oscillation signal is present and absent, for which the expected amplitude value is 1 and 0, respectively. Hypotheses for Δm_s associated with larger $\mathcal{A}$ values and smaller uncertainties $\sigma_{\mathcal{A}}$ in the scan contribute a larger weight in the fit.

The likelihood ratio (12.28) constitutes the Δm_s input to the CKM fit. This is illustrated for two study cases in Figure 12.1. The graphs representing (12.26) and (12.27) are also shown.

12.4 Posterior probability distributions

The global likelihood function (12.10) involves the product of terms corresponding to the individual constraints, which include $|V_{ub}/V_{cb}|$, $|\epsilon_K|$, $\sin 2\beta$, Δm_d and Δm_s. The likelihood may then be projected onto desired subspaces. The constraint on the apex of the unitarity triangle is achieved by performing the fit projection on the $(\bar{\rho}, \bar{\eta})$ space (12.12). As mentioned earlier, the projection over a given parameter or constraint variable is also achievable as (12.13) and (12.14) denote. The constraining power of a given constraint relation or input may be inspected by enabling and disabling it in the likelihood construction.

Firstly, we inspect the Δm_s posterior probability distribution for the case where the Δm_s information is disabled oi the fit. This is shown in Figure 12.2, yieding a favored 68% C.L. range given by $\Delta m_s \in (18.3, 23.8)\,\mathrm{ps}^{-1}$. It is interesting to note that the precise experimental measurement we have obtained falls near, though outside this expectation interval.

Next, we study the constraining effects obtained when using in the CKM fit the following two sets of information on Δm_s:

(A) the amplitude scan from Figure 8.8, which yields a *bound*, $\Delta m_s \in (16.6, 20.8)\,\mathrm{ps}^{-1}$ (at 95% C.L.), corresponding to the world average scan prior to the measurement, and

parameter	no Δm_s	Δm_s case A	Δm_s case B
Δm_s [ps^{-1}]	$21.1^{+2.8}_{-2.8}$	$20.0^{+1.0}_{-1.7}$	$17.4^{+0.3}_{-0.4}$
$\bar{\rho}$	$0.24^{+0.03}_{-0.03}$	$0.22^{+0.03}_{-0.04}$	$0.20^{+0.02}_{-0.02}$
$\bar{\eta}$	$0.35^{+0.03}_{-0.02}$	$0.35^{+0.03}_{-0.03}$	$0.36^{+0.02}_{-0.02}$
$\lvert V_{ub}/V_{cb}\rvert$	$0.010^{+0.005}_{-0.005}$	$0.010^{+0.005}_{-0.005}$	$0.010^{+0.001}_{-0.001}$
Δm_d [ps^{-1}]	$0.48^{+0.13}_{-0.13}$	$0.48^{+0.06}_{-0.12}$	$0.48^{+0.18}_{-0.20}$
$\sin 2\beta$	$0.76^{+0.02}_{-0.02}$	$0.76^{+0.02}_{-0.02}$	$0.77^{+0.03}_{-0.02}$
α [$^\circ$]	$103.0^{+7.4}_{-6.5}$	$98.9^{+4.6}_{-4.3}$	$98.5^{+7.0}_{-6.8}$
$\gamma[^o]$	$55.3^{+5.4}_{-5.7}$	$59.4^{+5.1}_{-3.9}$	$61.0^{+4.6}_{-4.0}$
R_b	$0.42^{+0.02}_{-0.02}$	$0.42^{+0.01}_{-0.01}$	$0.42^{+0.02}_{-0.01}$
R_t	$0.84^{+0.04}_{-0.04}$	$0.87^{+0.04}_{-0.03}$	$0.88^{+0.02}_{-0.02}$
B_K	$0.79^{+0.05}_{-0.04}$	$0.77^{+0.05}_{-0.05}$	$0.76^{+0.04}_{-0.04}$
$f_{B_d}\sqrt{B_{B_d}}$ [GeV]	$0.23^{+0.016}_{-0.02}$	$0.23^{+0.01}_{-0.02}$	$0.22^{+0.01}_{-0.02}$

Table 12.3: Output values of the *fitted* parameters, obtained without a Δm_s constraint, and with the two Δm_s constraints considered.

(B) the amplitude scan from Figure 10.3, which corresponds to the first direct *measurement* $\Delta m_s = 17.3^{+0.34}_{-0.19}\,\text{ps}^{-1}$.

This input information is represented in Figure 12.1. Clearly, the Δm_s information in case (B) is drastically better localized, with a stronger CKM parameter constraint being correspondingly anticipated.

The effects obtained with both sets of constraints are illustrated in the posterior probability distributions for Δm_s, $\bar{\rho}$, and $\bar{\eta}$ in Figure 12.3. In Figure 12.4 a representation of these effects is also provided in the $(\bar{\rho}, \bar{\eta})$ plane, where the various constraints employed in the fit are also represented. Table 12.3 displays the posterior fit resuts for various *fitted* parameters.

A significant shrinking of the confidence intervals for the CKM parameters, and for the apex of the unitarity triangle, is observed. It is verified also that, despite the fit preference for a slightly higher value of Δm_s, dictated by the other constraints interpreted within the standard model framework, the experimental measurement is otherwise finely accomodated.

12.5 Impact of the measurement

The CKM fitting framework that has been here assembled and used in the previous sections was originally prepared [86] to provide immediate feedback on the impact of the Δm_s measurements being pursued. More specifically, to allow a prompt estimation of the effect on the

determination of the unitarity triangle parameters in the standard model, and to dispose of a fully understood and flexible tool to perform tests of models beyond the standard model. Further details of additional studies performed are provided in [86]. Various other works readilly appeared in the literature inspecting the impact of the precise Δm_s measurement on various classes of flavor models [90].

Here we further present the outcome of the analysis of the impact of the ultimate Δm_s observation on the CKM global picture, evaluated using other, state-of-the-art CKM fitters. In particular, we refer for completeness to two standard implementations, one which is based also on Bayesian statistics [82] and one which is not [83]. For both cases, the results of the global fit performed before and after the Δm_s measurement are illustrated in Figures 12.5 and 12.6. The expected confidence intervals for Δm_s are also compared with the actual experimental measurement.

It is informative to also infer the ratio of the moduli of the CKM matrix elements V_{td} and V_{ts} directly, instead of doing so by using the corresponding constraint in the extensive CKM fit. This may be readily done using (2.56), to obtain

$$\left|\frac{V_{td}}{V_{ts}}\right| = \xi_\Delta \sqrt{\frac{\Delta m_d}{\Delta m_s}\,\frac{m_{B_s}}{m_{B^0}}} = 0.2060 \pm 0.0007^{+0.0081}_{-0.0060}\,. \tag{12.29}$$

In additions to the Δm_s measurement, the calculation uses as inputs $m_{B_s}/m_{B^0} = 0.98390 \pm \mathcal{O}(10^{-4})$ [87], $\Delta m_d = 0.507 \pm 0.005\,\mathrm{ps}^{-1}$ [88], and $\xi_\Delta = 1.21^{+0.047}_{-0.035}$ [89]. In (12.29) the first uncertainty refers to the contribution from the Δm_s measurement alone, while the second includes all other sources, dominated by the theoretical uncertainty on the parameter ξ_Δ. It is seen that the resolution on the experimental inputs contributes a negligible part to the total uncertainty, and that an improved determination of the parameter ξ_Δ from lattice calculations appears necessary in order to fully exploit the precision achieved in the Δm_s determination. The exquisite accuracy of the achieved Δm_s measurement can be further elucidated by comparing the relative precisions of the oscillation frequencies in the two B_s and B^0 neutral meson systems: $\sigma_{\Delta m_s}/\Delta m_s \sim 0.5\%$ surpassing $\sigma_{\Delta m_d}/\Delta m_d \sim 1\%$. The left plot of Figure 12.6 also shows a comparison of the precision achieved in the $|V_{td}/V_{ts}|$ determination, from the ratio of branching fraction measurements performed at the BaBar and Belle experiments, as well as from the global CKM fit.

Further analysis of the theoretical implications has also been extensively presented [90] and reviewed [91] elsewhere. The Δm_s precise measurement is observed to significantly constrain various classes of models, and to restrict the phase space, generically parameterized by h_s and σ_s in (2.73), of new physics contributions to the flavor sector.

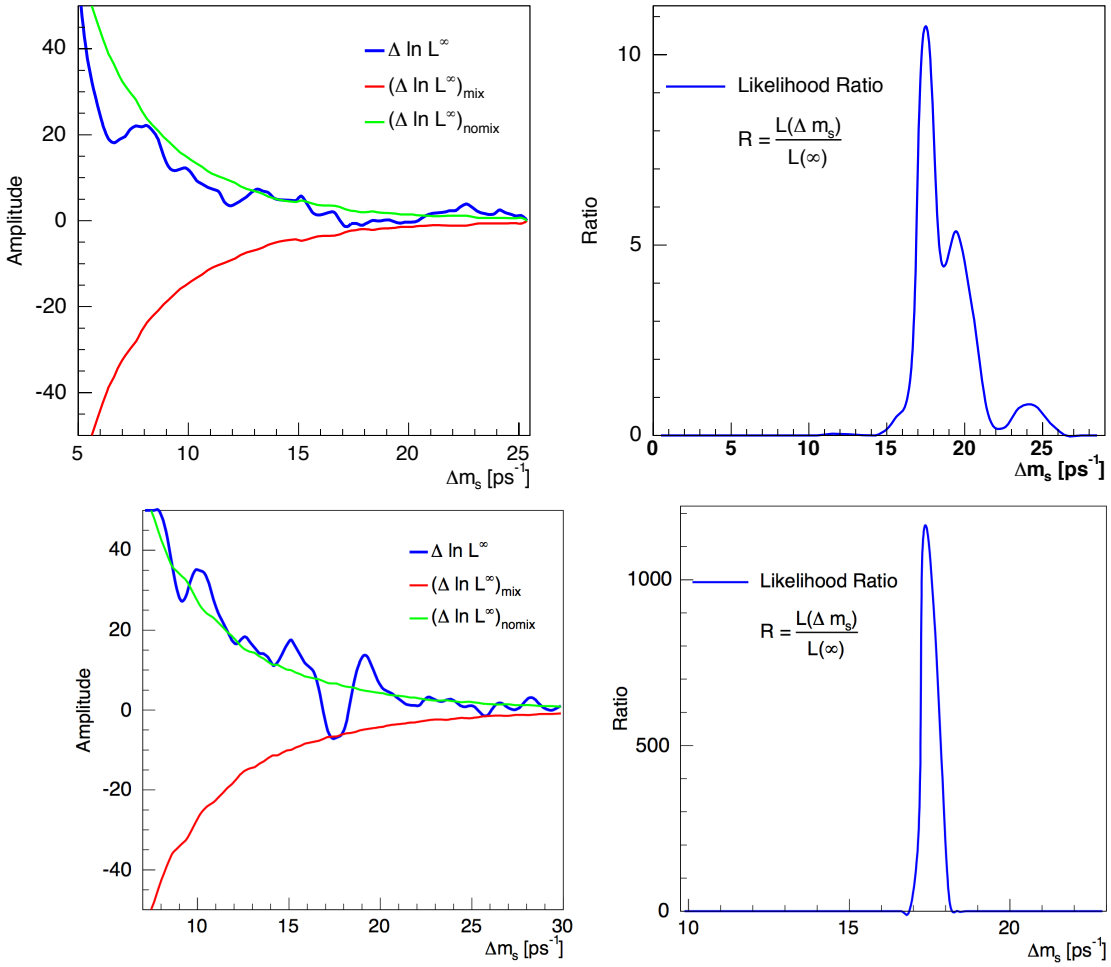

Figure 12.1: Delta log-likelihood (left) and likelihood ratio (right) distributions as a function of Δm_s , corresponding to the amplitude scans of Figure 8.8 (top) and of Figure 10.3 (bottom).

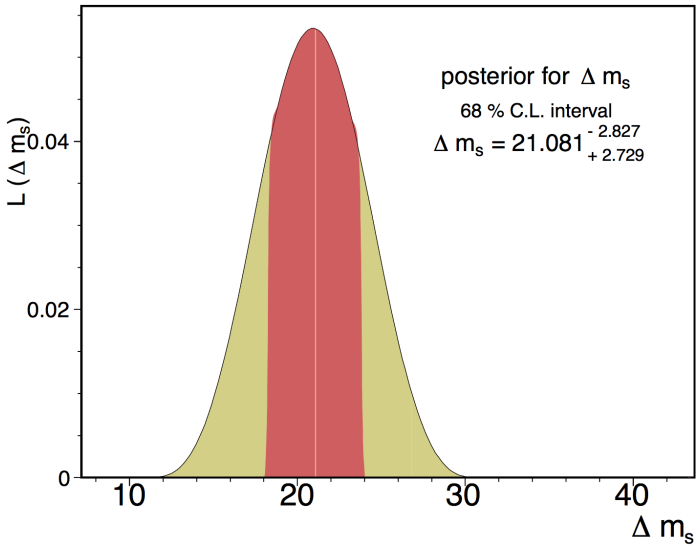

Figure 12.2: Posterior probability distributions for Δm_s obtained without the Δm_s constraint.

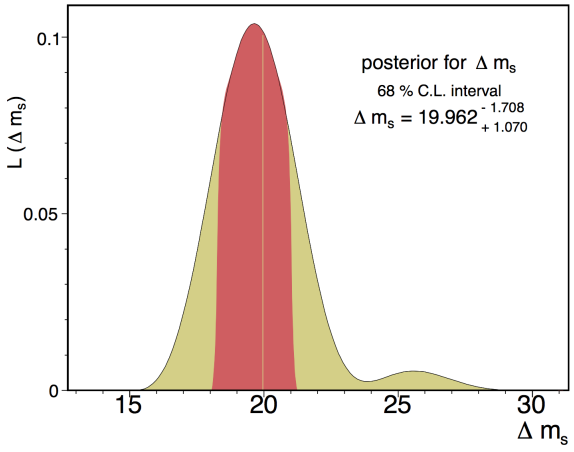

(a) Δm_s posterior with Δm_s constraint A (bound)

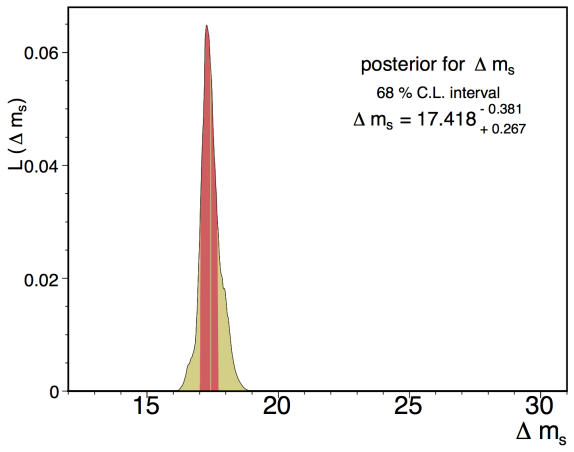

(b) Δm_s posterior with Δm_s constraint B (measurement)

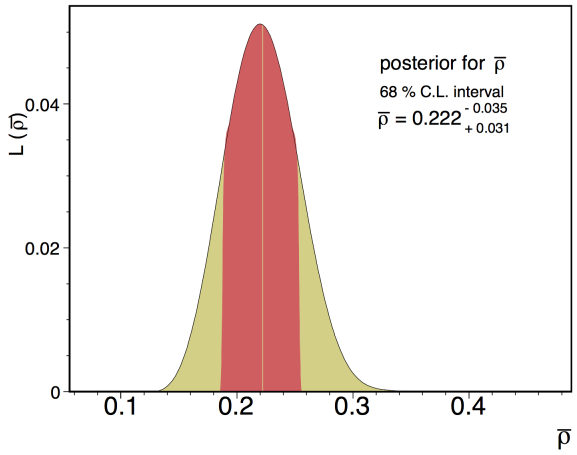

(c) $\bar{\rho}$ posterior with Δm_s constraint A (bound)

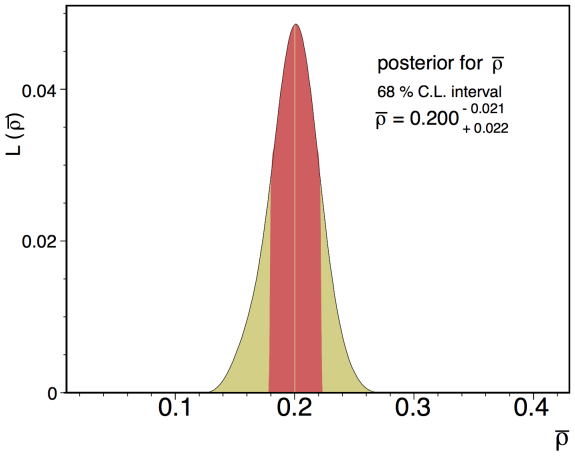

(d) $\bar{\rho}$ posterior with Δm_s constraint B (measurement)

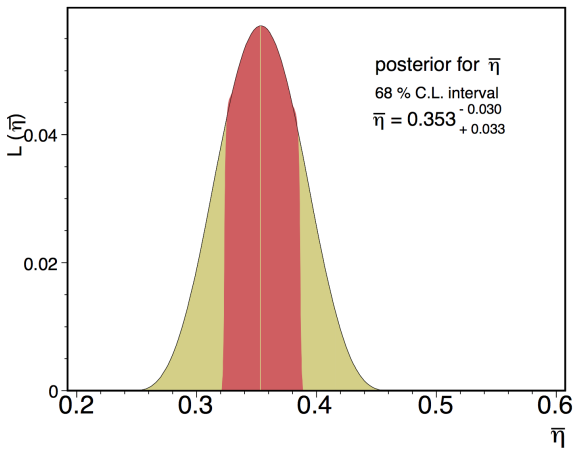

(e) $\bar{\eta}$ posterior with Δm_s constraint A (bound)

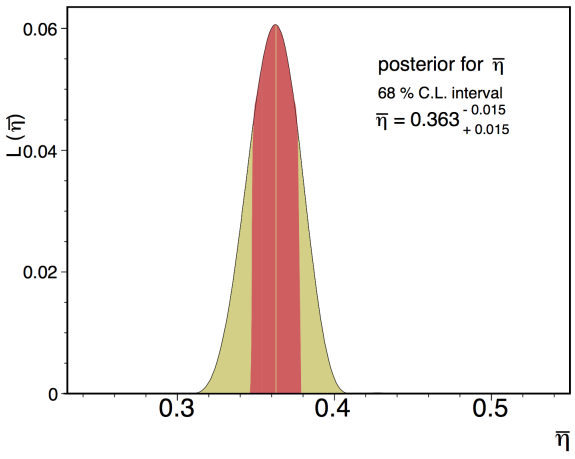

(f) $\bar{\eta}$ posterior with Δm_s constraint B (measurement)

Figure 12.3: Posterior probability distributions for Δm_s , $\bar{\rho}$, and $\bar{\eta}$.

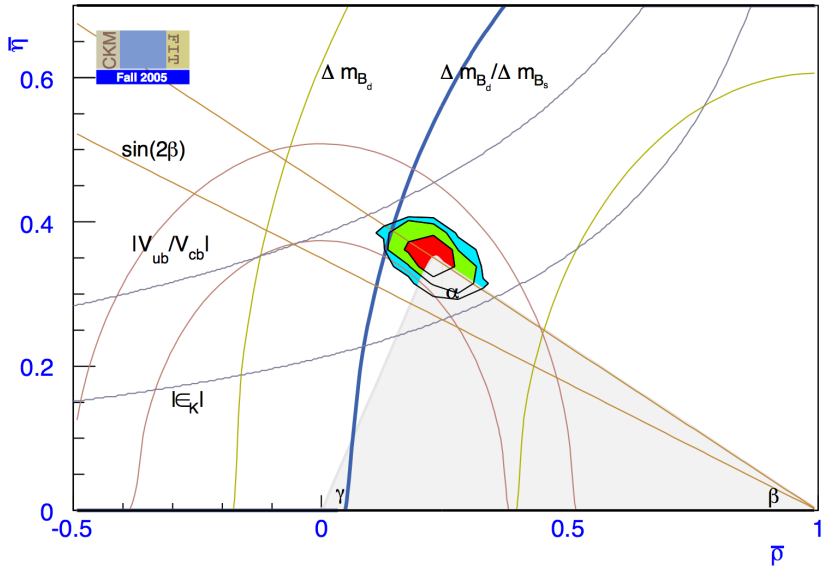

(a) $(\bar{\rho}, \bar{\eta})$ posterior with Δm_s constraint A (bound)

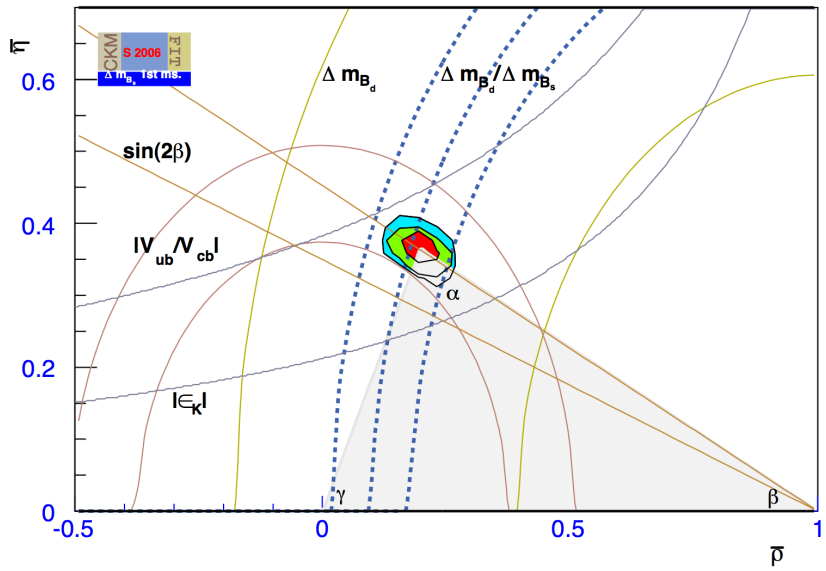

(b) $(\bar{\rho}, \bar{\eta})$ posterior with Δm_s constraint B (measurement)

Figure 12.4: Posterior probability distributions in the $(\bar{\rho}, \bar{\eta})$ plane.

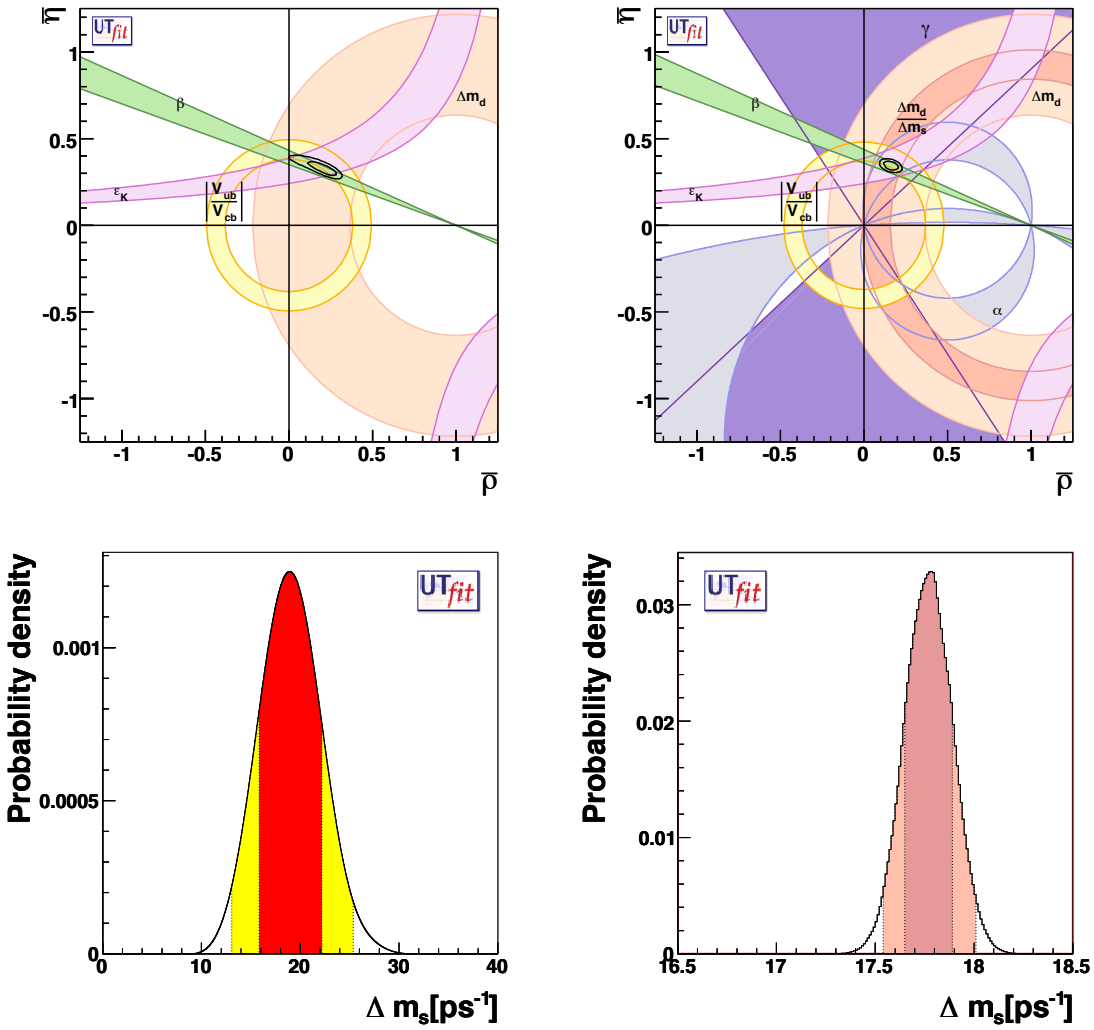

Figure 12.5: Posterior probability distributions calculated without Δm_s constraint (left) and including the Δm_s measurement (right) [82].

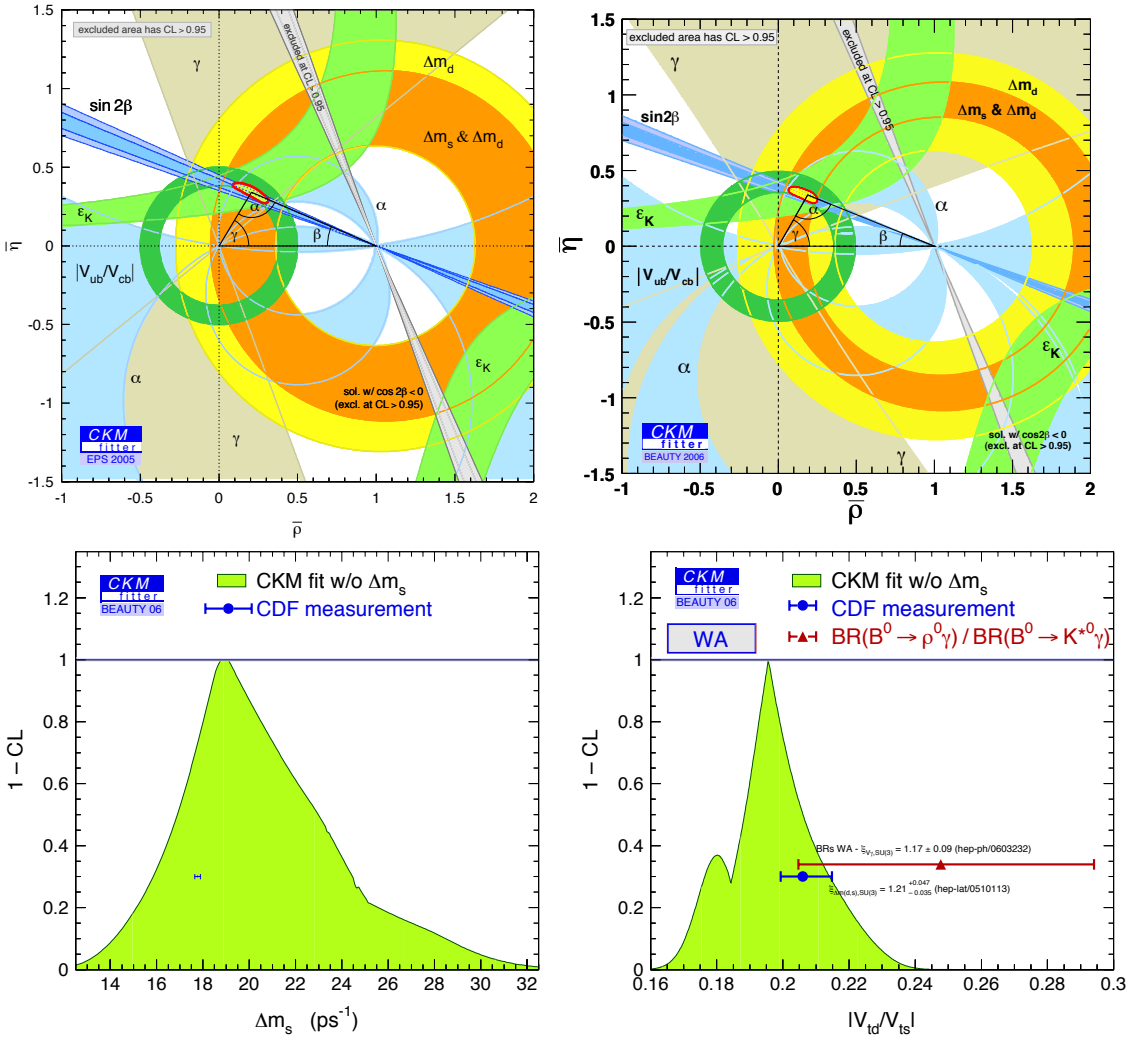

Figure 12.6: Comparison of the global CKM fit before (left) and after (right) the Δm_s measurement [83]. (Top) Confidence intervals projected on the $(\bar{\rho}, \bar{\eta})$ plane. (Bottom left) Comparison of the CKM fit expectation and the experimemtal Δm_s measurement; the latter is drawn at 1-C.L.=31.7% corresponding to a 1σ interval. (Bottom right) Comparison of the CKM fit expectation for $|V_{td}/V_{ts}|$, and determinations from the CDF Δm_s measurement and average Belle and BaBar measurements.

12.6 Résumé

An inference framework based on Bayesian statistics is implemented, and employed to constrain the CKM matrix parameters utilizing the Δm_s amplitude scan information, combined with other existing flavor-sector measurements and theoretical input.

The magnitude of the right side of the unitarity triangle is poorly known. Despite the high precision of the Δm_d measurement, the associated constraining power is limited by large theoretical uncertainties. A more powerful constraint is obtained with the inclusion of information about Δm_s, as the systematic uncertainty on the theoretical quantities involved in the ratio of the two oscillation frequencies is considerably reduced. The standard model expectation for Δm_s is inferred from a fit performed excluding the Δm_s input. The experimental measurement is found compatible with the region favored by the CKM fit. Nonetheless, the indirectly-derived (*i.e.* without using the Δm_s measurement itself as fit constraint) CKM confidence intervals are not constrained to a degree matching the precision of the experimental measurement, to yield a more conclusive test of the validity of the standard model of flavor interactions. In order to take the best advantage of the exquisite precision of the Δm_s experimental measurement, significant improvements in the lattice calculations become particularly relevant.

The impact of the Δm_s precise measurement on possible beyond the standard model contributions to the flavor sector has been also extensively investigated in the literature. The parameter space available for certain classes of models is found to be significantly restricted.